Journal of Biomechanics 97 (2019) 109348

Contents lists available at ScienceDirect

Journal of Biomechanics

journal homepage: www.elsevier.com/locate/jbiomech
www.JBiomech.com

Static optimization underestimates antagonist muscle activity at the glenohumeral joint: A musculoskeletal modeling study

Azadeh Kian [a], Claudio Pizzolato [b], Mark Halaki [c], Karen Ginn [d], David Lloyd [b], Darren Reed [d], David Ackland [a,*]

[a] Department of Biomedical Engineering, University of Melbourne, Australia
[b] GCORE, Menzies Health Institute Queensland and School of Allied Health Sciences, Griffith University, Australia
[c] Discipline of Exercise and Sport Science, Faculty of Health Sciences, The University of Sydney, Australia
[d] Discipline of Anatomy & Histology, Faculty of Medicine and Health, The University of Sydney, Australia

ARTICLE INFO

Article history:
Accepted 14 September 2019

Keywords:
Shoulder
Deltoid
Rotator cuff
EMG
Neuromusculoskeletal
Static optimization
Biomechanical model

ABSTRACT

Static optimization is commonly employed in musculoskeletal modeling to estimate muscle and joint loading; however, the ability of this approach to predict antagonist muscle activity at the shoulder is poorly understood. Antagonist muscles, which contribute negatively to a net joint moment, are known to be important for maintaining glenohumeral joint stability. This study aimed to compare muscle and joint force predictions from a subject-specific neuromusculoskeletal model of the shoulder driven entirely by measured muscle electromyography (EMG) data with those from a musculoskeletal model employing static optimization. Four healthy adults performed six sub-maximal upper-limb contractions including shoulder abduction, adduction, flexion, extension, internal rotation and external rotation. EMG data were simultaneously measured from 16 shoulder muscles using surface and intramuscular electrodes, and joint motion evaluated using video motion analysis. Muscle and joint forces were calculated using both a calibrated EMG-driven neuromusculoskeletal modeling framework, and musculoskeletal model simulations that employed static optimization. The EMG-driven model predicted antagonistic muscle function for pectoralis major, latissimus dorsi and teres major during abduction and flexion; supraspinatus during adduction; middle deltoid during extension; and subscapularis, pectoralis major and latissimus dorsi during external rotation. In contrast, static optimization neural solutions showed little or no recruitment of these muscles, and preferentially activated agonistic prime movers with large moment arms. As a consequence, glenohumeral joint force calculations varied substantially between models. The findings suggest that static optimization may under-estimate the activity of muscle antagonists, and therefore, their contribution to glenohumeral joint stability.

1. Introduction

The glenohumeral joint facilitates a large range of upper limb motion that is essential for performing many activities of daily living, including lifting, reaching, pushing and driving (Magermans et al., 2005). Stability of the glenohumeral is dependent on a balance of the individual forces and moments produced in the surrounding muscles to generate a net joint articular force that passes within the bounds of the glenoid fossa (Veeger and Van Der Helm, 2007). The simultaneous activity of the rotator cuff, and other muscles spanning the glenohumeral joint, compresses the humeral head into the concave glenoid fossa, thereby preventing anterior-posterior and superior-inferior joint translation. For example, during humeral abduction, deltoid generates an agonist elevation torque and superior-directed force, which combined with the antagonist torque and inferior-directed force of the inferior rotator cuff, results in a scapular-plane force couple that compresses the glenohumeral joint (Ackland and Pandy, 2009; Lucas, 1973). Similarly, humeral flexion and extension requires simultaneous activation of the anterior and posterior rotator cuff muscles to produce joint compression via a transverse-plane force couple (Rathi et al., 2016; Wattanaprakornkul et al., 2011). The role of the musculature in stabilizing the glenohumeral joint is clinically relevant, since muscle dysfunction can ultimately result in excessive joint shear, subluxation, pain and early-onset osteoarthritis (Yousif and Bicos, 2017). While several studies have advanced our understanding of muscle and joint loading at the shoulder (van der Helm and Veeger, 1996; Giroux and Lamontagne, 1992),

* Corresponding author at: Department of Biomedical Engineering, University of Melbourne, Parkville, Victoria 3010, Australia.
E-mail address: dackland@unimelb.edu.au (D. Ackland).

https://doi.org/10.1016/j.jbiomech.2019.109348
0021-9290/

there remains debate about the relative contributions of each shoulder muscle to net joint moments and glenohumeral joint articular forces. This is because shoulder muscle forces cannot be measured non-invasively, and the glenohumeral joint is a statically indeterminate system, which precludes calculation of a unique muscle force solution (An et al., 1984).

Computational models have been developed to estimate muscle and joint forces using numerical optimization subject to cost-functions that minimize the sum of squares of muscle stresses (Karlsson and Peterson, 1992; Charlton and Johnson, 2006; Nikooyan et al., 2011), muscle activations (Delp et al., 2007; Crowninshield and Brand, 1981; Kaufman et al., 1991), energy consumption (Praagman et al., 2006) and fatigue (Dul et al., 1984). These primarily estimate activation of agonist muscles (Yanagawa et al., 2008), but may not accurately predict the function of muscles that generate joint stiffness and are associated with dynamic stabilization, nor the motor recruitment strategies employed in cases of neuromuscular impairment. Musculoskeletal models that constrain the glenohumeral joint force to pass within the boundaries of the glenoid fossa have been shown to predict activity of the rotator cuff muscles during simulations of shoulder abduction (Van der Helm, 1994) and forward reaching (Dickerson et al., 2007); however, the capacity of this strategy to predict antagonist muscle function during activities of daily living is yet to be evaluated.

The use of electromyography (EMG) to drive simulations of movement using neuromusculoskeletal models is an alternative approach to quantifying muscle and joint loading that has been applied at the spine (Cholewicki et al., 1995; Gagnon et al., 2001), hip (Hoang et al., 2019, 2018), knee (Lloyd and Besier, 2003), ankle (Bogey et al., 2005; Manal et al., 2012), and elbow (Pau et al., 2012; Manal et al., 2002). EMG-driven modeling can account for subject-specific muscle recruitment strategies that are not mathematically constrained to specific cost functions (Buchanan et al., 2004; Sartori et al., 2012; Pizzolato et al., 2015). This is achieved by employing musculotendon and neural activation parameters calibrated to each subject, together with experimental measures of muscle activity to estimate musculotendon forces. Neuromusculoskeletal shoulder models driven from EMG recordings of each individual muscle have been challenging to develop due, in part, to the difficulties associated with recording EMG data from the extensive deep musculature using intramuscular electrodes. Hybrid neuromusculoskeletal shoulder models have been developed by utilizing EMG data from superficial muscles (Nikooyan et al., 2012), but these still require optimization and predictive functions to obtain a complete muscle force solution.

The aims of this study were twofold. First, to develop a neuromusculoskeletal model driven entirely from EMG data recorded from the major superficial and deep shoulder muscles; and second, to compare shoulder muscle and joint force predictions from the EMG-driven model with those calculated with static optimization using a musculoskeletal model of identical structure. It was hypothesized that the EMG-driven model would predict different muscle activity associated with the rotator cuff and prime-mover muscles than that obtained using static optimization. The findings will help elucidate the role of the shoulder musculature in glenohumeral joint stabilization, and in development of computational shoulder models.

2. Materials and methods

2.1. Subject recruitment

Four healthy adults (mean age ± one standard deviation: 25.0 ± 5.9 years; body mass: 65.9 ± 21.28 kg; height: 170.5 ± 11.21 cm; 3 female and 1 male) with no history of upper limb disease or previous surgery were recruited for testing (see Supplementary Material for further details). Ethical approval was obtained from The University of Sydney Human Research Ethics Committees and participants provided their written informed consent.

2.2. Subject testing protocol

Subjects were seated and performed, in random order, seven maximum voluntary contractions (MVCs) with their dominant limb, which included shoulder abduction, horizontal adduction, flexion, extension and internal rotation as well as elbow flexion and extension (Table 1). Each MVC task was performed against manual resistance and repeated three times (Ginn et al., 2011; Doheny et al., 2008; Jaskolska et al., 2006). Six isolated isometric ramp contractions were then undertaken at 50% maximal effort, specifically, abduction, adduction, flexion, extension, internal rotation and external rotation (Table 1). Each isometric contraction was performed by pulling a handle attached to a cord instrumented with a uniaxial load cell (Xtran, Applied Measurement,

Table 1
Upper limb maximum voluntary contractions and isometric contractions performed by each subject (Ginn et al., 2011; Doheny et al., 2008; Jaskolska et al., 2006). All isometric contractions were performed at 50% of the peak load generated during maximum isometric contractions.

	Task	Task Description
Maximum Voluntary Contraction	Shoulder abduction	Maximum shoulder abduction torque with the shoulder abducted to 90° in plane of scapula, the humerus internally rotated, and the elbow fully extended
	Shoulder horizontal adduction	Maximum shoulder horizontal adduction torque with both shoulders flexed to 90° and the elbows flexed to 20°, pressing the heel of the hands together
	Shoulder flexion	Maximum shoulder flexion torque with the shoulder flexed to 125° and the elbow fully extended
	Shoulder internal rotation	Maximum shoulder internal rotation torque with the shoulder abducted to 90° in plane of scapula and with neutral humeral rotation, and the elbow flexed to 90°
	Shoulder extension	Maximum shoulder extension torque with the arm by the side and shoulder abducted to 30° in the scapula plane
	Elbow flexion	Maximum elbow flexion torque with the shoulder positioned at 0° of flexion and the elbow flexed to 90°
	Elbow extension	Maximum elbow extensor torque with the shoulder positioned at 0° of flexion and the elbow flexed to 90°
Isometric Contraction	Shoulder flexion	Shoulder flexion with the shoulder in 90° of flexion and the forearm fully extended
	Shoulder extension	Shoulder extension with the shoulder flexed to 90° and the forearm fully extended
	Shoulder abduction	Shoulder abduction with the shoulder in 90° of abduction in scapular plane and the forearm fully extended
	Shoulder adduction	Shoulder adduction with the shoulder in 90° of abduction in scapular plane and the forearm fully extended
	Shoulder internal rotation	Shoulder internal rotation with the shoulder in 45° degrees of abduction and the elbow flexed to 90°
	Shoulder external rotation	Shoulder external rotation with the shoulder in 45° degrees of abduction and the elbow flexed to 90°

Australia). Trajectories of retro-reflective markers placed on the cord were measured using a 4-camera video motion analysis system (Vicon, UK) sampling at 120 Hz, and used to quantify the direction of the cord tension. Loading was maintained normal to the load-cell's sensing axis and perpendicular to each glenohumeral joint motion axis to ensure production of a pure joint moment, with non-prime joint moments considered negligible (<2% of net moment) and not analysed further. Each ramp contraction consisted of four seconds of gradual load increase to 50% maximal effort, three seconds of sustained contraction at 50% maximal effort, followed by four seconds of load decrease to resting level. The predefined ramp profile was based on the subject's maximum effort, which was determined with an MVC prior to testing. Subjects followed a visual trajectory of their contraction on a monitor to guide the execution of each contraction, and a minimum rest interval of one minute between tasks was provided. The chosen ramp profile was based on a pilot study that showed shorter ramp times lead to participants overshooting the 50% target, while longer times resulted in fatigue and long breaks.

During testing of each participant, EMG was measured from 16 shoulder muscles. Pairs of surface EMG electrodes (Red Dot, 2258, 3 M) were placed over pectoralis major, upper trapezius, lower trapezius, biceps brachii and triceps brachii following skin debridement and application of conducting gel (De Luca, 1997). Interelectrode distances were 20 mm, and skin impedance verified to be less than 5 kΩ (Day, 2002). Bipolar intramuscular (in-dwelling) electrodes were placed in anterior, middle and posterior deltoid sub-regions, rhomboid major, supraspinatus, infraspinatus, subscapularis, pectoralis minor, serratus anterior, teres major, and latissimus dorsi (Boettcher et al., 2008; Johnson et al., 2011; Ginn and Halaki, 2015), with ultrasonic guidance employed for rhomboid major and pectoralis minor electrode placement (Mindray, DP-9900). A ground electrode was placed on the contralateral acromion and scapular spine (Universal Electrosurgical Pad: Split, 9160F, Australia). Testing was undertaken over 2 days with one week between the test sessions. The functional tasks undertaken on each test day were identical, with the total number of intramuscular electrodes employed divided between the two test days. All EMG data were subsequently superimposed into one EMG superset. Common muscles tested on both days were used to verify the repeatability of the experimental protocol and EMG measurement (see Supplementary Material). EMG data were processed using a zero-lag, 8th order 10 Hz high-pass Butterworth filter, then full-wave rectified. Subsequent EMG linear envelopes were produced using a zero-lag 8th order 3 Hz low-pass Butterworth filter (Ginn et al., 2011). All EMG data were normalized to maximum values recorded from the MVC tasks.

Upper limb motion was simultaneously recorded during testing by tracking the trajectories of 15 retroreflective markers placed on the upper-limb using the video motion analysis system (Vicon, UK). The markers were placed according to a previously published upper limb markerset (Wu et al., 2016) (Fig. 1). Resultant marker trajectories were filtered using a fourth-order, zero-lag, 6 Hz low-pass Butterworth filter.

2.3. Musculoskeletal modeling

A 5-segment, 10 degree-of-freedom rigid-body musculoskeletal model of each subject's dominant upper limb was created in OpenSim by scaling a generic model to each subject's mass and anthropometry (Wu et al., 2016). The glenohumeral and acromioclavicular joints were modeled as 3-DOF constrained ball and socket joints, the sternoclavicular joint as a 2-DOF universal joint, and the forearm and wrist as one rigid segment that articulated with the elbow via a 2-DOF universal joint. The model was actuated by 23 Hill-type musculotendon units, which included 5 axiohumeral, 10 axioscapular and 8 scapulohumeral muscles and muscle sub-regions (Fig. 1). Each musculotendon unit's optimum muscle fibre length, l_o^m, and tendon slack length, l_s^t, were linearly scaled in equal proportion to match the scaled overall musculotendon unit length with the upper limb in the neutral position. Joint angles and moments for each sub-maximal isometric contraction were calculated using inverse kinematics and inverse dynamics, respectively.

Muscle forces were calculated using either static optimisation or calibrated EMG-driven modeling approaches, and the muscle forces then used to calculate glenohumeral joint forces. Employing a custom-developed Matlab plugin (Mathworks, MA, USA), the net joint moments were decomposed into muscle forces using static optimisation by minimising the sum of squared muscle activations (Wu et al., 2016). An anisotropic elliptical shape ratio constraint was applied between the compressive and shear components of the glenohumeral joint contact force, constraining the resultant glenohumeral joint force vector to pass within the articular boundary of the glenoid. Specifically, superior (F_s), anterior (F_a) and compressive components of the GH joint force (F_c) were computed and constrained using

$$\frac{F_s^2}{a^2}+\frac{F_a^2}{b^2}\le F_c^2 \tag{1}$$

where the constants a = 0.61 and b = 0.34 were derived previously (Lippitt and Matsen, 1993).

By implementing each subject's musculotendon shoulder models as used in static optimisation simulations, EMG-driven models were developed using the calibrated EMG-informed neuromusculoskeletal modeling toolbox (CEINMS) (Pizzolato et al., 2015). Each muscle's neural excitation was calculated from its pre-processed EMG signal using a second-order linear differential equation of backward differences (Thelen et al., 1994; Lloyd and Besier, 2003)

$$u(t)=\alpha e(t-d)-(C_1+C_2)u(t-1)-C_1.C_2u(t-2) \tag{2}$$

where $e(t)$ is the time-varying muscle excitation,$u(t)$ the neural excitation, d the electromechanical delay, α a muscle gain coefficient, and $C_1$and C_2 recursive coefficients (Lloyd and Besier, 2003). Muscle activation was modeled using a non-linear function of neural excitation (Lloyd and Besier, 2003)

$$a(t)=\frac{e^{A.u(t)}-1}{e^{A}-1} \tag{3}$$

where $a(t)$ is the time-varying muscle activation, $u(t)$ the time-varying neural excitation and A, a non-linear shape factor ranging between zero (a straight-line) and 3 (highly non-linear). Muscle forces were subsequently calculated using a Hill-type model of each musculotendon actuator

$$\begin{aligned}F^m(t)&=F^t(t)\\&=F^{max}\left[f_a(l_m)f_v(v_m).a(t)+f_p(l_m)+d_m.v_m\right].\cos\varphi\end{aligned} \tag{4}$$

where $F^m(t)$ is the time-varying force generated by the sum of muscle fibers, F^t the tendon force, F^{max} the maximum isometric muscle force,$f_a(l_m)$ the active force–length relation,$f_v(v_m)$ the muscle fibre contraction velocity relation, $f_p(l_m)$ the passive force- length relation, d_m a muscle damping coefficient, and φ the muscle pennation angle.

Each subject-specific EMG-driven neuromusculoskeletal model was calibrated over all sub-maximal contractions collected during the first test day. Specifically, the EMG-to-activation coefficients (C_1, C_2 and A) and musculotendon parameters (F^{max}, l_m^0, l_{st}) were adjusted using a simulated annealing algorithm to minimize errors between joint moments calculated from inverse dynamics and those generated by muscles using the EMG-driven neuromuscu-

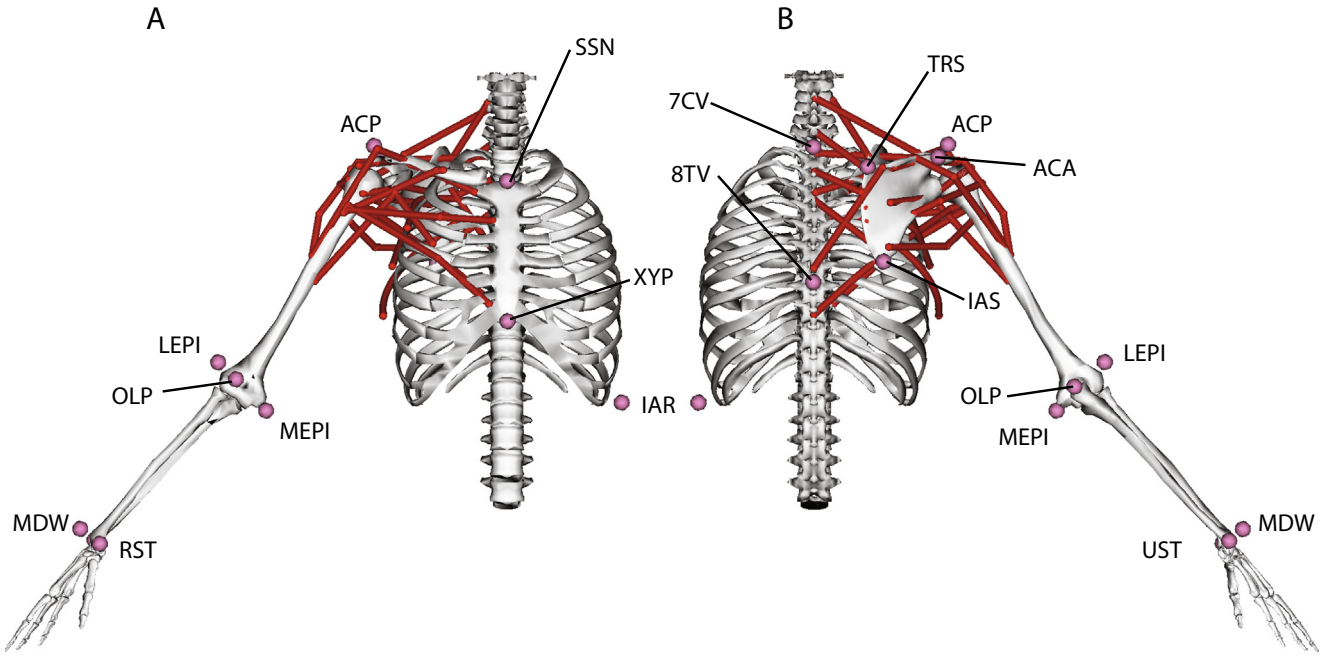

Fig. 1. Anterior view (A) and posterior view (B) of neuromusculoskeletal upper limb model structure employed in the present study. Displayed are the major musculotendon actuators (red lines) and markerset adopted. Symbol definitions are as follows: MEPI, medial epicondyle; LEPI, lateral epicondyle; OLP, olecranon process; RST, radial styloid of wrist; MDW, mid-dorsal region of wrist; OST, ulna styloid of wrist; IAR, inferior aspect of 11th rib; 7CV, 7th cervical vertebra; 8TV, 8th thoracic vertebra; SSN, suprasternal notch; XYP, xyphoid process; ACP, acromion process; IAS, inferior angle of scapula; ACA, acromial angle; TRS, trigonum spinae. For descriptions of musculotendon actuators, see Wu et al. (2016). (For interpretation of the references to colour in this figure legend, the reader is referred to the web version of this article.)

loskeletal model (see Supplementary Material). This was achieved by mapping the EMG from the 16 muscles to the 23 musculotendon units in the model, with the EMG of multi-sub-region muscles distributed in proportion to their volume across the separate musculotendon units representing each sub-region. The calibrated EMG-driven neuromusculoskeletal model was then used to calculate musculotendon and joint forces using the combined EMG-data and joint kinematics for each sub-maximal isometric contraction without use of static optimisation or implementation of a glenohumeral joint force constraint. Shoulder joint contact forces were determined using the same approach as for static optimisation. Predictions of muscle and joint forces and muscle-generated torques between the EMG-driven neuromusculoskeletal model and the static optimization-based models were calculated. Results were reported for selected muscles known to have an important role in glenohumeral joint actuation and stability (Wu et al., 2016, 2017, 2018). EMG data and computed model outputs were expressed as a percentage of task duration, and all forces express as a percentage of body weight (%BW). Standard deviation between subjects was used as a measure of data dispersion.

3. Results

3.1. Abduction

For the isometric abduction tasks, the EMG-driven neuromusculoskeletal model predicted that anterior deltoid, middle deltoid, supraspinatus and infraspinatus were agonists (contributing abduction torque), while latissimus dorsi, pectoralis major and teres major were antagonists (contributing adduction torque) (Fig. 2C). In contrast, static optimization predicted antagonist function in subscapularis (Table 2). Both models predicted antagonistic function in the posterior deltoid and supraspinatus, but these muscles made negligible contributions to the net joint moment. The EMG-driven model predicted more force in anterior deltoid (78.5 ± 34.3%BW) than middle deltoid (52.1 ± 21.0%BW), in contrast to static optimisation estimates of 25.4 ± 4.8%BW and 65.3 ± 13.1%BW for anterior and middle deltoid, respectively (Table 3). The EMG-driven model also predicted a lower mean peak subscapularis force (7.8 ± 8.2%BW) compared with that predicted by static optimisation (44.9 ± 8.0%BW). Similarly, muscle recruitment predicted using the EMG-driven model and static optimization during flexion and extension were shown to vary substantially (see Supplementary Material). The EMG-driven and static optimisation model demonstrated similar peak glenohumeral joint force magnitudes during isometric abduction (139.9 ± 48.6%BW and 139.7 ± 26.5%BW, respectively), but different anterior-posterior shear force directions (Fig. 2D).

3.2. Adduction

For the isometric adduction tasks, the EMG-driven model showed that latissimus dorsi, teres major and pectoralis major were active agonists, while anterior deltoid, middle deltoid, supraspinatus and infraspinatus were antagonists (Fig. 3C). Static optimization predicted similar levels of antagonist function in infraspinatus, but lower in anterior and middle deltoid (Table 2). Both models showed posterior deltoid and subscapularis to be an antagonist and agonist, respectively; however, their contributions to the net joint moment were extremely small. EMG-driven modeling predicted a maximum teres major force of 16.5 ± 10.0%BW, while static optimization predicted negligible force generation from this muscle, with similar trends observed with middle deltoid and supraspinatus. Peak glenohumeral joint force magnitude predictions were similar between EMG-driven model (83.5 ± 25.4% BW) and static optimization solutions (72.3 ± 13.6%BW), although, static optimization produced joint shear of opposite direction to that of the EMG-driven model (Table 3).

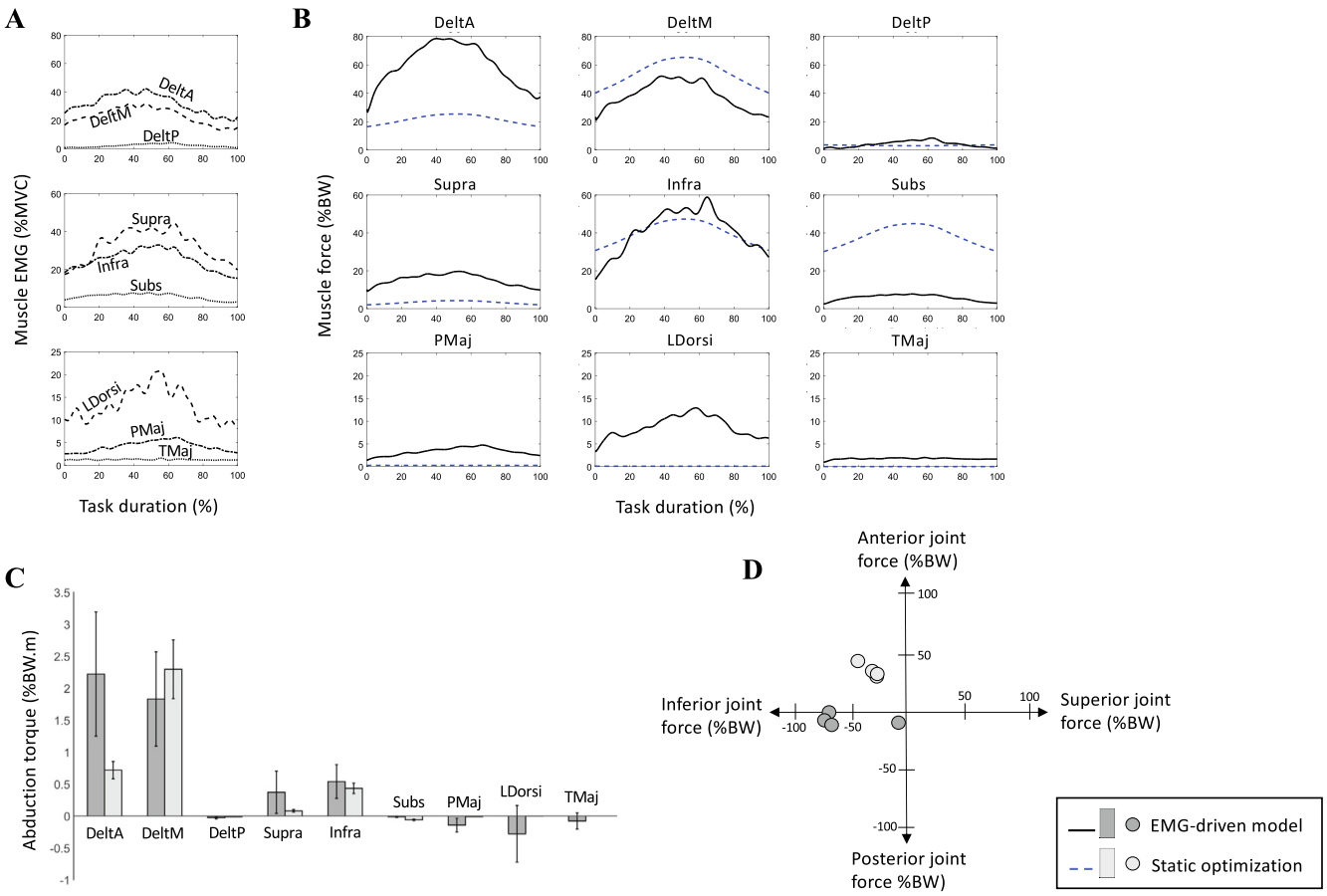

Fig. 2. Mean data during isometric abduction including EMG (A), muscle and joint forces calculated using the EMG-driven neuromusculoskeletal model and static optimization (B) muscle contributions to the maximum net joint moment calculated using the EMG-driven model and static optimization (C), and glenohumeral joint force components at the maximum joint moment calculated using the EMG-driven model and static optimization for each of the four subjects (D). Data are displayed for nine selected muscles including the anterior deltoid (DeltA), middle deltoid (DeltM), posterior deltoid (DeltP), supraspinatus (Supra), infraspinatus (Infra), subscapularis (Subs), pectoralis major (PMaj), latissimus dorsi (LDorsi) and teres major (TMaj). A positive moment represents abduction, while a negative moment represents adduction.

Table 2
Mean and standard deviation (SD) of individual muscle contributions to maximum net joint moments calculated during isometric abduction, adduction, flexion, extension, internal rotation, and external rotation using the EMG-driven neuromusculoskeletal model (NM) and static optimization (SO). All data are expressed in %BW.m.

	Abduction				Adduction				Flexion				Extension				Internal rotation				External rotation			
	NM		SO		NM		SO		NM		SO		NM		SO		NM		SO		NM		SO	
	Mean	SD	Mean	SD	Mean	SD	Mean	SD	Mean	SD	Mean	SD	Mean	SD	Mean	SD	Mean	SD	Mean	SD	Mean	SD	Mean	SD
Anterior deltoid	2.22	0.97	0.72	0.14	0.16	0.03	0.07	0.07	2.33	1.97	1.95	0.70	0.11	0.03	0.10	0.12	0.00	0.00	−0.01	0.00	−0.01	0.00	−0.01	0.00
Middle deltoid	1.83	0.74	2.30	0.46	0.17	0.09	0.05	0.06	0.99	0.71	0.43	0.13	0.29	0.22	0.05	0.03	0.00	0.00	0.00	0.00	−0.04	0.01	−0.04	0.01
Posterior deltoid	−0.03	0.02	−0.01	0.00	0.03	0.02	0.01	0.00	−0.27	0.20	−0.06	0.00	−0.99	0.55	−1.98	0.29	−0.05	0.04	−0.10	0.04	−0.09	0.05	0.00	0.00
Supraspinatus	0.37	0.33	0.08	0.02	0.16	0.18	0.00	0.00	0.34	0.36	0.34	0.11	0.22	0.31	0.62	0.08	−0.04	0.04	0.00	0.00	−0.10	0.08	−0.09	0.03
Infraspinatus	0.54	0.27	0.43	0.08	0.13	0.11	0.14	0.02	0.87	0.62	0.60	0.23	0.10	0.10	0.57	0.09	−0.06	0.07	−0.48	0.13	−1.59	0.92	−0.96	0.33
Subscapularis	−0.01	0.01	−0.06	0.01	−0.02	0.01	−0.02	0.00	−0.01	0.01	−0.01	0.00	0.11	0.03	0.55	0.08	0.39	0.40	1.86	0.88	0.23	0.31	0.04	0.03
Pectoralis major	−0.14	0.11	−0.01	0.00	−0.09	0.08	−0.01	0.00	−0.31	0.07	0.00	0.00	−0.05	0.03	0.00	0.00	0.05	0.03	0.01	0.00	0.05	0.05	0.00	0.00
Latissimus dorsi	−0.28	0.44	0.00	0.00	−0.80	0.32	−0.67	0.15	−0.44	0.59	0.00	0.00	−0.54	0.38	−0.58	0.11	0.26	0.23	0.27	0.28	0.16	0.24	0.00	0.00
Teres major	−0.08	0.13	0.00	0.00	−0.59	0.36	−0.12	0.03	−0.22	0.23	0.00	0.00	−0.49	0.26	−0.59	0.09	0.06	0.04	0.00	0.00	0.02	0.03	0.00	0.00

3.3. Internal rotation

For the isometric internal rotation tasks, EMG-driven modeling showed that subscapularis, latissimus dorsi, teres major and pectoralis major were agonists, while infraspinatus and posterior deltoid behaved as weak antagonists (Fig. 4C). Static optimization recruited the subscapularis and latissimus dorsi as agonists, and infraspinatus and posterior deltoid as antagonists (Table 2). Both models predicted that anterior and middle deltoid and supraspinatus were antagonists that contributed very little to the net joint moment. The EMG-driven model calculated a mean peak middle deltoid force of 21.0 ± 9.5%BW, while static optimization predicted minimal middle deltoid force generation (Table 3). Similarly, the EMG-driven model calculated a maximum teres major force of 8.6 ± 6.2%BW; however, static optimization predicted no activity in this muscle. In contrast, the mean maximum subscapularis force calculated using static optimization was 81.8 ± 38.9%BW, while that estimated using the EMG-driven model was 17.1 ± 17.8%BW. The peak glenohumeral joint force magnitude estimated using static optimization and

Table 3
Mean and standard deviation (SD) of the peak muscle and joint forces calculated during isometric abduction, adduction, flexion, extension, internal rotation, and external rotation using the EMG-driven neuromusculoskeletal model (NM) and static optimization (SO). All data are given at the point of maximum glenohumeral joint force magnitude for each task and expressed as a percentage of body weight (%BW).

	Abduction				Adduction				Flexion				Extension				Internal rotation				External rotation			
	NM		SO		NM		SO		NM		SO		NM		SO		NM		SO		NM		SO	
Muscle Forces	Mean	SD	Mean	SD	Mean	SD	Mean	SD	Mean	SD	Mean	SD	Mean	SD	Mean	SD	Mean	SD	Mean	SD	Mean	SD	Mean	SD
Anterior deltoid	78.5	34.3	25.4	4.8	6.3	1.3	2.6	2.6	61.0	51.6	51.1	18.4	3.1	0.7	2.7	3.3	20.7	11.7	23.1	2.7	25.0	6.3	24.8	7.3
Middle deltoid	52.1	21.0	65.3	13.1	5.1	2.6	1.6	1.8	32.9	23.6	14.3	4.5	11.5	9.0	2.1	1.4	21.0	9.5	2.6	4.1	23.6	8.9	26.4	6.8
Posterior deltoid	8.5	5.7	3.6	0.2	17.4	11.5	5.5	0.6	12.2	9.1	2.8	0.2	33.2	18.6	66.4	9.9	11.9	9.2	24.2	9.4	12.9	7.3	0.2	0.0
Supraspinatus	19.7	17.5	4.3	1.1	9.3	10.6	0.1	0.0	13.1	13.9	13.2	4.4	9.0	12.6	25.2	3.4	6.7	7.6	0.3	0.0	24.8	19.3	21.6	7.5
Infraspinatus	58.9	28.9	47.3	8.9	17.8	14.5	19.4	3.2	72.0	51.4	49.4	18.7	12.5	12.4	70.9	10.6	3.0	3.5	22.6	6.3	77.1	44.5	46.3	15.8
Subscapularis	7.8	8.2	44.9	8.0	14.6	10.9	16.1	1.9	10.8	14.3	16.2	3.9	14.2	3.2	69.3	9.7	17.1	17.8	81.8	38.9	9.6	13.2	1.6	1.1
Middle pectoralis major	4.8	3.6	0.3	0.0	2.9	2.6	0.3	0.0	11.6	2.6	0.1	0.0	2.1	1.3	0.1	0.0	3.1	1.8	0.5	0.0	3.3	3.2	0.2	0.0
Latissimus dorsi	12.9	20.6	0.1	0.0	41.7	16.8	35.0	7.6	18.2	24.2	0.1	0.0	27.0	19.0	29.1	5.5	14.8	13.2	15.2	16.1	10.9	16.6	0.1	0.0
Teres major	2.0	3.3	0.0	0.0	16.5	10.0	3.3	0.7	4.9	5.1	0.0	0.0	10.6	5.5	12.6	1.9	8.6	6.2	0.0	0.0	3.0	4.2	0.0	0.0
Glenohumeral joint force																								
Compressive	127.6	42.4	128.8	24.2	74.7	22.4	67.4	12.5	223.1	10.6	162.1	59.6	85.6	28.7	221.5	32.5	69.6	14.3	109.9	49.9	97.7	37.2	123.8	56.4
Anterior	−8.7	5.6	38.1	6.9	−18.1	18.6	21.2	3.8	34.4	30.8	27.0	7.7	21.1	18.2	73.4	10.8	−13.5	7.0	37.1	16.6	−38.1	28.0	28.1	12.4
Superior	−53.7	31.5	−38.7	8.1	26.6	16.4	−15.3	3.6	40.9	6.8	−86.2	33.9	44.3	12.0	30.5	4.4	−19.4	13.9	3.7	9.4	21.7	25.4	−56.2	26.3
Magnitude	139.9	48.6	139.7	26.5	83.5	25.4	72.3	13.6	231.1	5.7	185.6	68.9	99.8	31.6	235.3	34.5	75.1	11.7	116.2	53.0	110.1	43.9	138.9	63.5

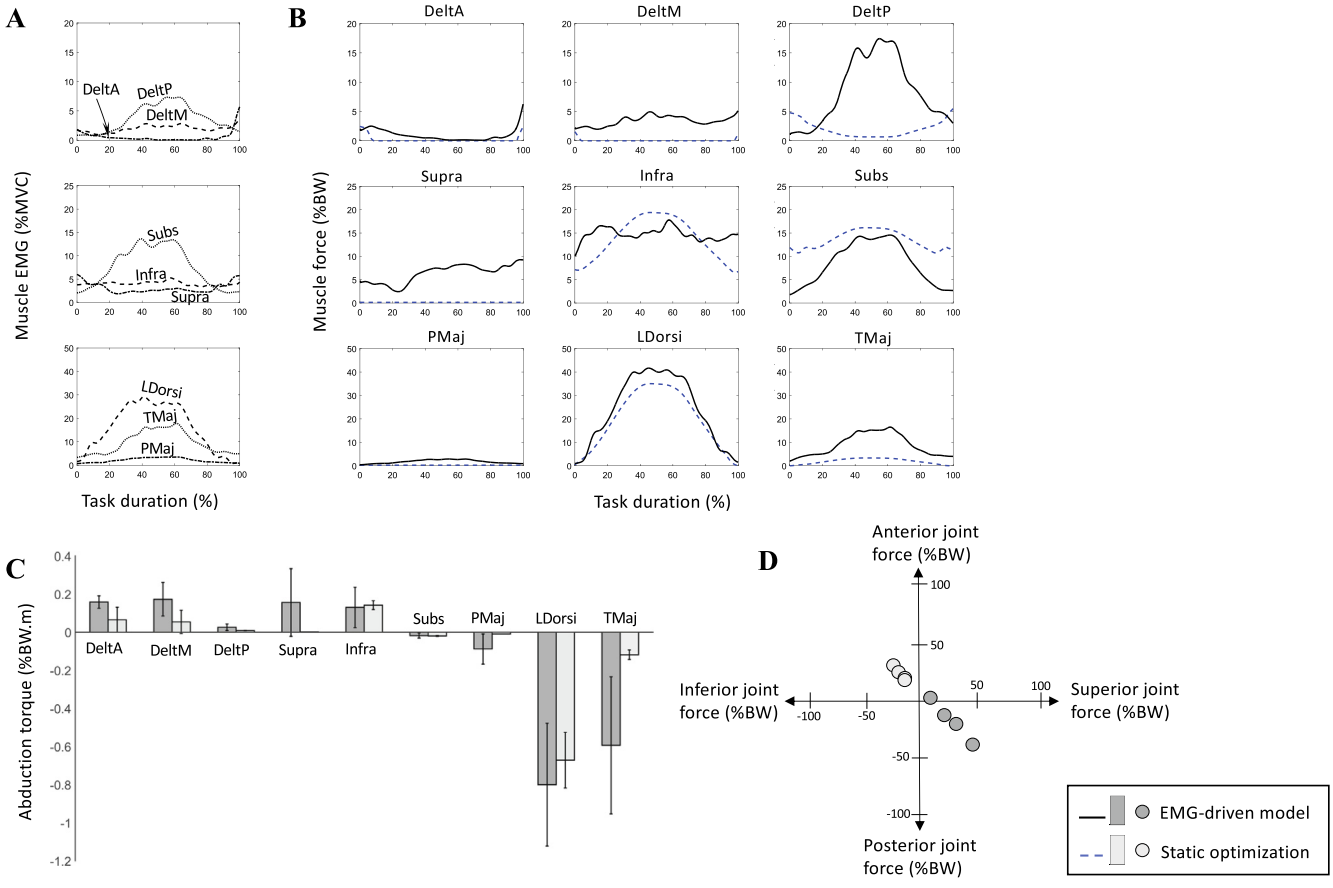

Fig. 3. Mean data during isometric adduction including EMG (A), muscle and joint forces calculated using the EMG-driven neuromusculoskeletal model and static optimization (B) muscle contributions to the maximum net joint moment calculated using the EMG-driven model and static optimization (C), and glenohumeral joint force components at the maximum joint moment calculated using the EMG-driven model and static optimization for each of the four subjects (D). Data are displayed for nine selected muscles. For muscle definitions, see caption of Fig. 2. A positive moment represents abduction, while a negative moment represents adduction.

the EMG-driven models were 116.2 ± 53.0%BW and 75.1 ± 11.7% BW, respectively. Static optimization predicted anterior joint force shear, while the EMG-driven model estimated posterior joint shear.

3.4. External rotation

For the isometric external rotation tasks, EMG-driven modeling recruited infraspinatus as the major agonist, while supraspinatus,

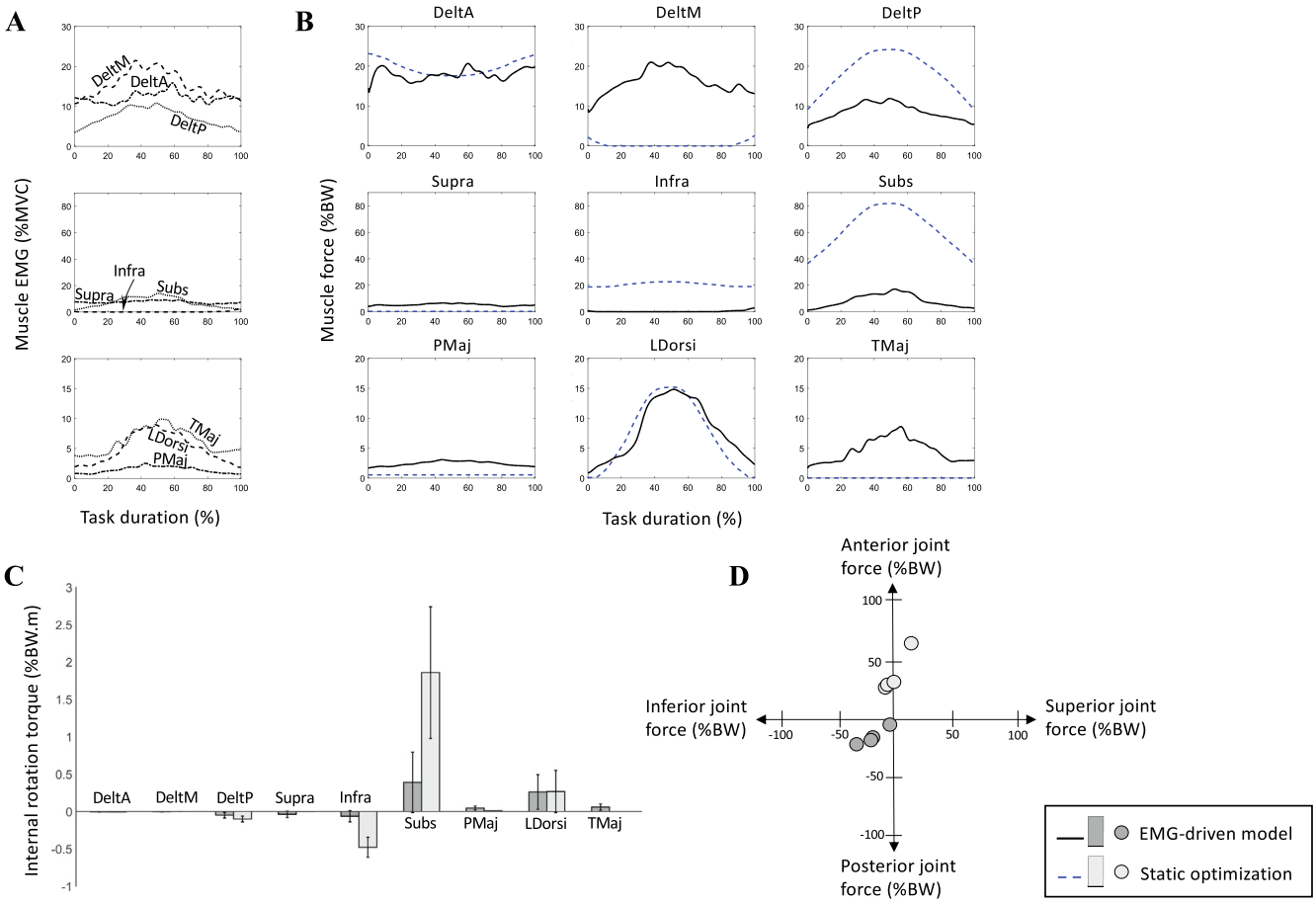

Fig. 4. Mean data during isometric internal rotation including EMG (A), muscle and joint forces calculated using the EMG-driven neuromusculoskeletal model and static optimization (B) muscle contributions to the maximum net joint moment calculated using the EMG-driven model and static optimization (C), and glenohumeral joint force components at the maximum joint moment calculated using the EMG-driven model and static optimization for each of the four subjects (D). Data are displayed for nine selected muscles. For muscle definitions, see caption of Fig. 2. A positive moment represents internal rotation, while a negative moment represents external rotation.

and all deltoid subregions were weak agonists, and subscapularis, latissimus dorsi, pectoralis major and teres major antagonists (Fig. 5C). There were no muscles recruited as external rotation antagonists using static optimization (Table 2). Static optimization predicted little force generation in posterior deltoid (0.2 ± 0.0% BW), while the EMG-driven model predicted a peak posterior deltoid force of 12.9 ± 7.3%BW (Table 3). In external rotation tasks, EMG-driven modeling and static optimization predicted a glenohumeral joint force peak of 110.1 ± 43.9%BW and 138.9 ± 63.5% BW, respectively. EMG-driven modeling calculated superior and posterior glenohumeral joint shear, while static optimization predicted inferior and anterior joint shear.

4. Discussion

The results of the present study provide strong evidence in support of the hypothesis that EMG-driven models and static optimization predict different muscle activity associated with the rotator cuff and prime-mover muscles. For example, the RMS differences in muscle forces between static optimization and EMG-driven neuromusculoskeletal model estimates were 19.1%BW, 5.6%BW, 21.0%BW and 8.0%BW for abduction, adduction, internal rotation and external rotation, respectively. Static optimization preferentially recruited large volume prime mover muscles with large lever arms, such as deltoid and latissimus dorsi, which was inconsistent with EMG and the EMG-driven neuromusculoskeletal modeling results (Ackland et al., 2008; Ackland and Pandy, 2011). Recruitment of muscles with large torque capacity is a hallmark of the static optimization objective function to minimize the sum of squared muscle activations, and has been demonstrated previously (Wu et al., 2016; Van der Helm, 1994). For example, middle deltoid and supraspinatus had peak abduction moment arms of 29.6 mm and 12.1 mm, respectively, and while the EMG-driven model recruited both middle deltoid and supraspinatus during isometric abduction, the static optimization solution predicted negligible force in supraspinatus (Fig. 3B). Thus, while static optimization may provide reasonable estimates of prime-mover muscle contributions to net joint moments, the EMG data and results of EMG-driven modeling in the present study suggest static optimization may underestimate activity of muscles with small leverage.

The EMG-driven model predicted antagonist muscle function during isometric abduction and flexion in pectoralis major, latissimus dorsi and teres major. While the peak EMG measurements in some of these muscles were low (<5%MVC), the cumulative torque contribution of the antagonist muscles is likely to play an important role in glenohumeral joint stabilization. Importantly, the EMG-driven modeling glenohumeral joint force passed within the boundaries of the glenoid without use of a constraint function for abduction and flexion, as well as adduction and internal rotation. Active shoulder elevation requires considerable antagonist muscle activity to balance the prominent superior shear force generated by deltoid due to its large volume, force capacity and superior inclination (Ackland and Pandy, 2009). The present study demonstrates that at 90° of abduction, antagonist muscle function

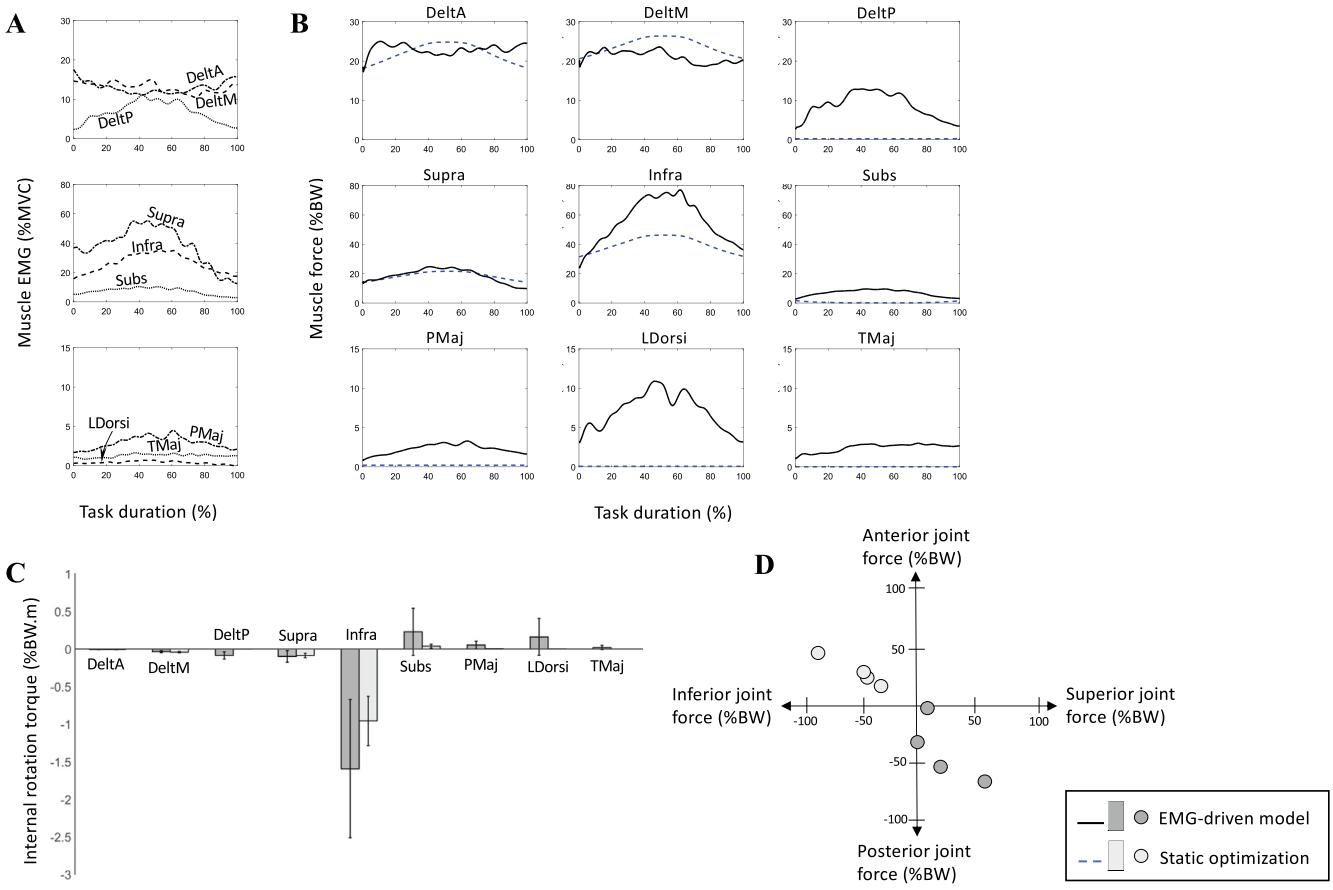

Fig. 5. Mean data during isometric external rotation including EMG (A), muscle and joint forces calculated using the EMG-driven neuromusculoskeletal model and static optimization (B) muscle contributions to the maximum net joint moment calculated using the EMG-driven model and static optimization (C), and glenohumeral joint force components at the maximum joint moment calculated using the EMG-driven model and static optimization for each of the four subjects (D). Data are displayed for nine selected muscles. For muscle definitions, see caption of Fig. 2. A positive moment represents internal rotation, while a negative moment represents external rotation.

is predominantly achieved by the combined action of the subscapularis as well as latissimus dorsi and teres major, the latter of which are large muscles that insert below the neck of the humerus and have substantial humeral depressor leverage.

When decomposing net shoulder joint moments into muscle forces using static optimization, it has been shown that a constraint on the glenohumeral joint force direction is required to simulate activation in the rotator cuff muscles (Wu et al., 2016). While our static optimization simulations used a previously established function to constrain the ratio of shear to compression produced by the shoulder musculature (Lippitt and Matsen, 1993), the resultant rotator cuff muscle activity was at times inconsistent with the measured EMG and EMG-driven modeling data. For instance, during isometric external rotation the neuromusculoskeletal model estimated a mean subscapularis force peak of 9.6 ± 13.9%BW, and the peak subscapularis EMG was 10.5%MVC, yet static optimization predicted negligible activity in this muscle (Table 3). These findings suggest that detailed numerical models of personalised muscle recruitment may be required for predicting antagonistic muscle activity and quantifying each muscle's contributions to glenohumeral joint stability.

The present study showed that the varying muscle activation patterns calculated using the EMG-driven neuromusculoskeletal model and static optimisation solutions resulted in markedly different predictions of glenohumeral joint force direction. For example, during isometric adduction the neuromusculoskeletal model calculated a glenohumeral joint force with superior and posterior shear components, while static optimization predicted anterior and inferior joint shear force (Fig. 3). This discrepancy may be due to the absence of substantial middle deltoid and supraspinatus force generation in static optimization calculations, which would otherwise have the potential to contribute superior and posterior glenohumeral joint shear (Ackland and Pandy, 2009).

The present study has some limitations. First, the static optimization modeling assumed rigid tendons, while the EMG-driven neuromusculoskeletal model had passive elastic tendons; however, estimation of muscle forces assuming stiff and compliant tendons have been shown to produce similar results. Millard et al., (2013) reported large errors with high ratios of optimal fibre lengths and tendon slack lengths, but this had minimal effect at sub-maximal activation levels. For the musculoskeletal models in the present study, optimum fibre lengths and tendon slack lengths were initially tuned to ensure muscles operated on the ascending limb and around the peak of the muscle force-length curve, thus reducing the effect of passive force. Second, the objective of the present study was to compare muscle and joint force predictions from an EMG-driven model with those of a non-EMG-based static optimization model. Because calibration was not undertaken with the static optimisation model, musculotendon parameters may have varied between models, influencing muscle and joint force predictions. Therefore, static optimization solutions with and without musculotendon parameter calibration were also explored (see Supplementary Material for a comparison). Third, there may have been some differences in each subject's isometric contractions between test days, though contractions were standardized by visually following a ramp profile in real-time, and EMG measured from

common muscles on both test days showed high levels of agreement (see Supplementary Material). Fourth, low level activity recorded from muscles with intramuscular electrodes may be due to pain, and not directly associated with the motor task tested (Farina et al., 2004). Finally, a small sample size was employed in the study design, and this resulted in large standard deviations of EMG-driven model outputs because of between-subject variations in measured muscle EMG. However, strong trends were observed across all subjects and used to derive the study conclusions, including differences in model predictions of muscle onset and offset. Comparison of muscle-generated net joint moments using the EMG-driven neuromusculoskeletal model with inverse dynamics joint moments also showed a high level of agreement in most tasks (see Supplementary Material). Furthermore, we have shown high agreement between glenohumeral joint force magnitudes calculated using the EMG-driven model compared with those measured using an instrumented implant (see Supplementary Material).

5. Conclusion

In conclusion, EMG-driven neuromusculoskeletal modelling demonstrated antagonist muscle function at the shoulder that was not predicted using static optimization. This was characterized by activation and force generation by the pectoralis major, latissimus dorsi and teres major during abduction and flexion, supraspinatus during adduction, middle deltoid during extension, and subscapularis, pectoralis major and latissimus dorsi during external rotation. As a consequence, glenohumeral joint force direction varied substantially between the neuromusculoskeletal model and static estimation-based calculations. While the measured EMG activity of some antagonist muscles was low (<5% MVC), the combined contribution of all anatagonist muscles to net joint moments suggests co-contraction as a means for generating joint compression and therefore stability. The findings highlight limitations in the use of static optimization for predicting muscle function at the shoulder. Specifically, static optimization may be useful in estimating agonistic shoulder muscle force but may not provide accurate subject-specific estimations of antagonistic muscle activity associated with glenohumeral stabilising function. The results may be useful in development and interpretation of computational models of the upper limb.

Declaration of Competing Interest

The authors do not have any financial or personal relationships with other people or organizations that could inappropriately influence this manuscript.

Acknowledgements

This project was partially funded through ARC Industry Transformation Training Centre in Medical Implant Technologies (IC180100024).

Appendix A. Supplementary material

Supplementary data to this article can be found online at https://doi.org/10.1016/j.jbiomech.2019.109348.

References

Ackland, D.C., Pak, P., Richardson, M., Pandy, M.G., 2008. Moment arms of the muscles crossing the anatomical shoulder. J. Anatomy 213 (4), 383–390.
Ackland, D.C., Pandy, M.G., 2009. Lines of action and stabilizing potential of the shoulder musculature. J. Anatomy 215 (2), 184–197.
Ackland, D.C., Pandy, M.G., 2011. Moment arms of the shoulder muscles during axial rotation. J. Orthop. Res. 29 (5), 658–667.
An, K.N., Kwak, B.M., Chao, E.Y., Morrey, B.F., 1984. Determination of muscle and joint forces: a new technique to solve the indeterminate problem. J. Biomech. Eng. 106 (4), 364–367.
Bergmann, G., Graichen, F., Bender, A., Kääb, M., Rohlmann, A., Westerhoff, P., 2007. In vivo glenohumeral contact forces—measurements in the first patient 7 months postoperatively. J. Biomech. 40 (10), 2139–2149.
Boettcher, C.E., Ginn, K.A., Cathers, I., 2008. Standard maximum isometric voluntary contraction tests for normalizing shoulder muscle EMG. J. Orthop. Res. 26 (12), 1591–1597.
Bogey, R., Perry, J., Gitter, A., 2005. An EMG-to-force processing approach for determining ankle muscle forces during normal human gait. IEEE Trans. Neural Syst. Rehab. Eng. 13 (3), 302–310.
Buchanan, T.S., Lloyd, D.G., Manal, K., Besier, T.F., 2004. Neuromusculoskeletal modeling: estimation of muscle forces and joint moments and movements from measurements of neural command. J. Appl. Biomech. 20 (4), 367–395.
Charlton, I.W., Johnson, G., 2006. A model for the prediction of the forces at the glenohumeral joint. Proc. Inst. Mech. Eng., Part H: J. Eng. Med. 220 (8), 801–812.
Cholewicki, J., McGill, S.M., Norman, R.W., 1995. Comparison of muscle forces and joint load from an optimization and EMG assisted lumbar spine model: towards development of a hybrid approach. J. Biomech. 28 (3), 321–325.
Corana, A., Marchesi, M., Martini, C., Ridella, S., 1987. Minimizing multimodal functions of continuous variables with the "simulated annealing" algorithm Corrigenda for this article is available here. ACM Trans. Math. Software (TOMS) 13 (3), 262–280.
Crowninshield, R.D., Brand, R.A., 1981. A physiologically based criterion of muscle force prediction in locomotion. J. Biomech. 14 (11), 793–801.
Day, S., 2002. Important Factors in Surface EMG Measurement. Bortec Biomedical Ltd publishers, pp. 1–17.
De Luca, C.J., 1997. The use of surface electromyography in biomechanics. J. Appl. Biomech. 13 (2), 135–163.
Delp, S.L., Anderson, F.C., Arnold, A.S., Loan, P., Habib, A., John, C.T., Guendelman, E., Thelen, D.G., 2007. OpenSim: open-source software to create and analyze dynamic simulations of movement. IEEE Trans. Biomed. Eng. 54 (11), 1940–1950.
Dickerson, C.R., Chaffin, D.B., Hughes, R.E., 2007. A mathematical musculoskeletal shoulder model for proactive ergonomic analysis. Comput. Methods Biomech. Biomed. Eng. 10 (6), 389–400.
Doheny, E.P., Lowery, M.M., FitzPatrick, D.P., O'Malley, M.J., 2008. Effect of elbow joint angle on force–EMG relationships in human elbow flexor and extensor muscles. J. Electromyogr. Kinesiol. 18 (5), 760–770.
Dul, J., Townsend, M., Shiavi, R., Johnson, G., 1984. Muscular synergism—I. On criteria for load sharing between synergistic muscles. J. Biomech. 17 (9), 663–673.
Farina, D., Arendt-Nielsen, L., Merletti, R., Graven-Nielsen, T., 2004. Effect of experimental muscle pain on motor unit firing rate and conduction velocity. J. Neurophysiol. 91 (3), 1250–1259.
Gagnon, D., Lariviere, C., Loisel, P., 2001. Comparative ability of EMG, optimization, and hybrid modelling approaches to predict trunk muscle forces and lumbar spine loading during dynamic sagittal plane lifting. Clin. Biomech. 16 (5), 359–372.
Ginn, K., Halaki, M., Cathers, I., 2011. Revision of the shoulder normalization tests is required to include rhomboid major and teres major. J. Orthop. Res. 29 (12), 1846–1849.
Ginn, K.A., Halaki, M., 2015. Do surface electrode recordings validly represent latissimus dorsi activation patterns during shoulder tasks?. J. Electromyogr. Kinesiol. 25 (1), 8–13.
Giroux, B., Lamontagne, M., 1992. Net shoulder joint moment and muscular activity during light weight-handling at different displacements and frequencies. Ergonomics 35 (4), 385–403.
Hoang, H.X., Diamond, L.E., Lloyd, D.G., Pizzolato, C., 2019. A calibrated EMG-informed neuromusculoskeletal model can appropriately account for muscle co-contraction in the estimation of hip joint contact forces in people with hip osteoarthritis. J. Biomech. 83, 134–142.
Hoang, H.X., Pizzolato, C., Diamond, L.E., Lloyd, D.G., 2018. Subject-specific calibration of neuromuscular parameters enables neuromusculoskeletal models to estimate physiologically plausible hip joint contact forces in healthy adults. J. Biomech. 80, 111–120.
Jaskolska, A., Kisiel-Sajewicz, K., Brzenczek-Owczarzak, W., Yue, G.H., Jaskolski, A., 2006. EMG and MMG of agonist and antagonist muscles as a function of age and joint angle. J. Electromyogr. Kinesiol. 16 (1), 89–102.
Johnson, V.L., Halaki, M., Ginn, K.A., 2011. The use of surface electrodes to record infraspinatus activity is not valid at low infraspinatus activation levels. J. Electromyogr. Kinesiol. 21 (1), 112–118.
Karlsson, D., Peterson, B., 1992. Towards a model for force predictions in the human shoulder. J. Biomech. 25 (2), 189–199.
Kaufman, K.R., An, K.W., Litchy, W.J., Chao, E.Y., 1991. Physiological prediction of muscle forces–I. Theoretical formulation. Neuroscience 40 (3), 781–792.
Lippitt, S., Matsen, F., 1993. Mechanisms of glenohumeral joint stability. Clin. Orthop. Related Res. 291, 20–28.
Lloyd, D.G., Besier, T.F., 2003. An EMG-driven musculoskeletal model to estimate muscle forces and knee joint moments in vivo. J. Biomech. 36 (6), 765–776.
Lucas, D.B., 1973. Biomechanics of the shoulder joint. Arch. Surgery 107 (3), 425–432.

Magermans, D., Chadwick, E., Veeger, H., Van Der Helm, F., 2005. Requirements for upper extremity motions during activities of daily living. Clin. Biomech. 20 (6), 591–599.
Manal, K., Gonzalez, R.V., Lloyd, D.G., Buchanan, T.S., 2002. A real-time EMG-driven virtual arm. Comput. Biol. Med. 32 (1), 25–36.
Manal, K., Gravare-Silbernagel, K., Buchanan, T.S., 2012. A real-time EMG-driven musculoskeletal model of the ankle. Multibody Syst. Dynam. 28 (1–2), 169–180.
Millard, M., Uchida, T., Seth, A., Delp, S.L., 2013. Flexing computational muscle: modeling and simulation of musculotendon dynamics. J. Biomech. Eng. 135 (2), 021005.
Nikooyan, A., Veeger, H., Westerhoff, P., Bolsterlee, B., Graichen, F., Bergmann, G., Van der Helm, F., 2012. An EMG-driven musculoskeletal model of the shoulder. Human Movement Sci. 31 (2), 429–447.
Nikooyan, A., Veeger, H., Westerhoff, P., Graichen, F., Bergmann, G., Van der Helm, F., 2010. Validation of the Delft shoulder and Elbow model using in-vivo glenohumeral joint contact forces. J. Biomech. 43 (15), 3007–3014.
Nikooyan, A.A., Veeger, H.E., Chadwick, E.K., Praagman, M., Helm, F.C., 2011. Development of a comprehensive musculoskeletal model of the shoulder and elbow. Med. Biol. Eng. Comput. 49 (12), 1425–1435.
Pau, J.W., Xie, S.S., Pullan, A.J., 2012. Neuromuscular interfacing: establishing an EMG-driven model for the human elbow joint. IEEE Trans. Biomed. Eng. 59 (9), 2586–2593.
Pizzolato, C., Lloyd, D.G., Sartori, M., Ceseracciu, E., Besier, T.F., Fregly, B.J., Reggiani, M., 2015. CEINMS: a toolbox to investigate the influence of different neural control solutions on the prediction of muscle excitation and joint moments during dynamic motor tasks. J. Biomech. 48 (14), 3929–3936.
Praagman, M., Chadwick, E., Van Der Helm, F., Veeger, H., 2006. The relationship between two different mechanical cost functions and muscle oxygen consumption. J. Biomech. 39 (4), 758–765.
Rathi, S., Taylor, N.F., Green, R.A., 2016. The effect of in vivo rotator cuff muscle contraction on glenohumeral joint translation: an ultrasonographic and electromyographic study. J. Biomech. 49 (16), 3840–3847.
Sartori, M., Reggiani, M., Farina, D., Lloyd, D.G., 2012. EMG-driven forward-dynamic estimation of muscle force and joint moment about multiple degrees of freedom in the human lower extremity. PloS one 7 (12), e52618.
Thelen, D.G., Schultz, A.B., Fassois, S.D., Ashton-Miller, J.A., 1994. Identification of dynamic myoelectric signal-to-force models during isometric lumbar muscle contractions. J. Biomech. 27 (7), 907–919.
Van der Helm, F.C., 1994. A finite element musculoskeletal model of the shoulder mechanism. J. Biomech. 27 (5), 555–569.
van der Helm, F.C., Veeger, H.E., 1996. Quasi-static analysis of muscle forces in the shoulder mechanism during wheelchair propulsion. J. Biomech. 29 (1), 39–52.
Veeger, H., Van Der Helm, F., 2007. Shoulder function: the perfect compromise between mobility and stability. J. Biomech. 40 (10), 2119–2129.
Wattanaprakornkul, D., Cathers, I., Halaki, M., Ginn, K.A., 2011. The rotator cuff muscles have a direction specific recruitment pattern during shoulder flexion and extension exercises. J. Sci. Med. Sport 14 (5), 376–382.
Wu, W., Fong, J., Crocher, V., Lee, P.V.S., Oetomo, D., Tan, Y., Ackland, D.C., 2018. Modulation of shoulder muscle and joint function using a powered upper-limb exoskeleton. J. Biomech. 72, 7–16.
Wu, W., Lee, P.V., Ackland, D.C., 2017. The sensitivity of shoulder muscle and joint force predictions to changes in joint kinematics: a Monte-Carlo analysis. Gait Posture 54, 87–92.
Wu, W., Lee, P.V., Bryant, A.L., Galea, M., Ackland, D.C., 2016. Subject-specific musculoskeletal modeling in the evaluation of shoulder muscle and joint function. J. Biomech. 49 (15), 3626–3634.
Yanagawa, T., Goodwin, C.J., Shelburne, K.B., Giphart, J.E., Torry, M.R., Pandy, M.G., 2008. Contributions of the individual muscles of the shoulder to glenohumeral joint stability during abduction. J. Biomech. Eng. 130 (2), 021024.
Yousif, M.J., Bicos, J., 2017. Biomechanical comparison of single- versus double-row capsulolabral repair for shoulder instability: a review. Orthop. J. Sports Med. 5 (12). 2325967117742355.